

# Design of Access-Tube TDR Sensor for Soil Water Content: Theory

Joaquin J. Casanova, *Member, IEEE*, Steven R. Evett, and Robert C. Schwartz

**Abstract**—Soil water measurement is important in water management for irrigation and hydrologic sciences. The purpose of this paper is to describe the design of a cylindrical access-tube mounted waveguide for use in time-domain reflectometry (TDR) for *in-situ* soil water content sensing. In order to optimize the design with respect to sampling volume and losses, we derived the electromagnetic fields produced by a TDR sensor with this geometry. Using this analytical derivation, the effects on sampling area, waveform shape, and losses while varying design and soil water content were examined. It was found that when the soil and tube substrate have identical dielectrics, then sampling area has a local extremum. Tube radius has the largest impact of any geometrical parameter on sampling area with increases in radius causing increases in sampling area. Increasing electrode separation angle increases the sampling area slightly. The effects on TDR waveform are greatest for soil water content, tube dielectric, and tube radius: where increasing any of these increase delay and dispersion.

**Index Terms**—Dielectric, electromagnetics, sensors, soil water.

## I. INTRODUCTION

**K**NOWLEDGE of soil water content in the root zone is vital for management of (irrigation) water available to crops. The recent movement towards scheduling irrigation to supply water to crops at near optimal or deficit conditions requires water content sensors with improved accuracies [1]. Many methods have been explored for sensing soil water content, including remotely, by passive microwave sensing [2] and *in-situ*, by neutron thermalization, capacitance probes, or time-domain reflectometry probes [3]. Neutron probes are impractical due to the regulatory burden and the fact that they cannot be left unattended for data logging. Capacitance probes suffer inaccuracies due to soil conductivity, temperature effects and variations in response due to variations in soil structure [4]–[6]. Time domain reflectometry (TDR) uses the travel time of a pulse sent down a waveguide surrounded by the medium to be measured [7]. The travel time is related to the soil dielectric permittivity, which in turn is related to the

soil water content. TDR designs have been explored including printed circuit board [8], trifilar rod probes [9], and cylindrical access-tube designs [10]. However, TDR sensing of soil water content presents three main problems. First, the dispersive nature of the soil medium distorts the transmitted waveform, usually a rectangular pulse. The transmitted pulse has spectral content over a broad bandwidth; since the permittivity of many soils are strongly frequency-dependent, the different frequency components propagate with different velocities, resulting in a distorted reflected waveform that is difficult to interpret [11]. Second, probes that include some plastic layer in addition to the conductive elements measure a permittivity that is a combination of the soil permittivity and the permittivity of the probe body. The sampling area of the probe gives an indication of the fraction of the field penetrating into the soil and probe dielectric. This makes it difficult to translate the measured permittivity into a soil water content. Third, the soil medium is lossy, particularly at high frequencies, which can make waveform interpretation difficult.

To overcome these difficulties, various approaches on the circuit side of the design could be considered, such as shorting diodes [12] or frequency-domain techniques [13]. Also, the sensor design could be optimized with respect to probe geometry. Using computer-aided engineering (CAE) is one approach to optimizing the sensor shape [14]. In general, the CAE design approach consists of several steps. First, parameterize the design, that is, describe the geometry and material properties in terms of variables to be optimized. Second, model the relevant physical quantities, such as electromagnetic fields, then calculate an objective function that reflects the design objectives. Finally, optimize the design by maximizing the objective function through variation of the design parameters. This approach has been used successfully in the past for electromagnetic design in a wireless power transfer system [15]. This paper comprises the first of two investigating the performance of a particular sensor geometry. This paper seeks to describe the fields given a particular sensor geometry. Later, this solution could be used in a design optimization. The second paper investigates the performance of actual sensors in different media, including soil.

For electromagnetic modeling of TDR probes, some have examined the probes as waveguides in theory, using the assumption of transverse electromagnetic (TEM) mode propagation analytically [16] or numerically [17], showing some relationship of probe geometry and variation in the spatial distribution of the permittivity to sampling area [18]–[21]. However, TEM propagation is unrealistic for a TDR probe that incorporates some plastic coating or plastic substrate,

Manuscript received July 12, 2011; revised November 16, 2011; accepted December 9, 2011. Date of publication December 22, 2011; date of current version April 25, 2012. This work was supported in part by the Ogallala Aquifer Program, a consortium between USDA-Agricultural Research Service, Kansas State University, Texas AgriLife Research, Texas AgriLife Extension Service, Texas Tech University, and West Texas A&M University. The associate editor coordinating the review of this paper and approving it for publication was Dr. Dwight L. Woolard.

The authors are with the USDA-ARS CPRL, Bushland, TX 79012 USA (e-mail: joaquin.casanova@ars.usda.gov; steve.evett@ars.usda.gov; robert.schwartz@ars.usda.gov).

Color versions of one or more of the figures in this paper are available online at <http://ieeexplore.ieee.org>.

Digital Object Identifier 10.1109/JSEN.2011.2181354

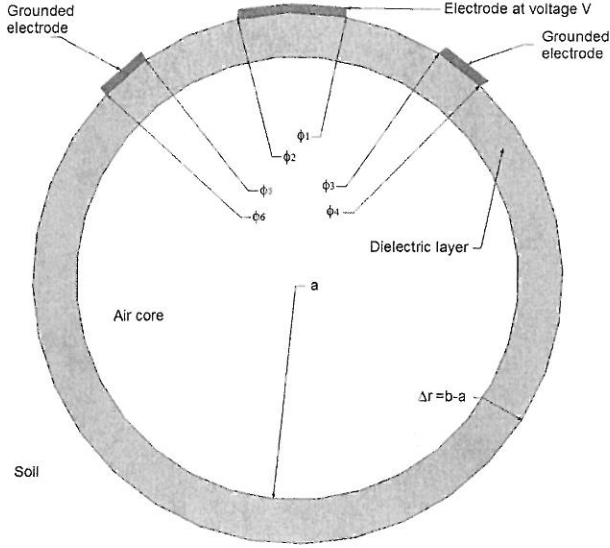


Fig. 1. Probe cross-section and parameterization.  $z$  (propagation) direction is into the page.

due to the boundary conditions on continuous tangential field components at the material interfaces [22]. A mode that is applicable to the cylindrical access-tube design is the family of hybrid modes [23], which is the typical treatment for open-boundary rod waveguides such as fiber optic cables. The case of a hollow optical fiber was treated analytically in [24].

In this paper, the fields are first derived analytically, assuming hybrid mode propagation. Using the derived fields, and the soil dielectric model in [25], the effects of probe geometry and soil water content on waveform shape and probe sensitivity to soil dielectric are investigated.

#### A. Access Tube Design and Geometrical Parameterization

Fig. 1 shows a cross-section of the probe design with design parameters. The waveguide-on-access-tube TDR design consists of a cylindrical plastic tube, such as PVC, with three electrodes on its surface that may or may not be connected to voltage ground or a source voltage. The probe can be fully described by the following variables: Probe length, tube inner radius  $a$ , thickness  $\Delta r$  (or outer radius  $b$ ), tube dielectric value  $\epsilon$ , electrode width and electrode spacing (or positions  $\phi_i$ ). For the sake of brevity, we only consider an annulus with an air core; we don't discuss the possible case of a metal layer on the interior of the tube, although this is another option in the design.

## II. THEORY

Maxwell's equations can be solved analytically using various degrees of simplifying assumptions. For all analytical solution techniques, boundary conditions and sources must be incorporated. The enforcement of boundary conditions results in a nonlinear, implicit characteristic equation, the solution of which yields the significant at each frequency [22]. The sources are incorporated by using a Fourier-Bessel expansion [26]. These steps are the most difficult and must be done

numerically. So any analytical approach used in estimating the fields for the probe is really a quasi-analytical approach. The quasi-analytical, frequency domain technique was used for EM design optimization with success in [15], therefore it is the primary approach used here. The TEM [16], [27] has been used before. The quasi-TEM solution would be less valid as the difference between the permittivities increases, because the difference between the tangential field components in the different media at the material interfaces would be more pronounced. Since the permittivity of the soil can take a very broad range while the tube dielectric is fixed, it seems to be an unrealistic assumption. The most physically realistic for this open boundary waveguide is the family of hybrid modes.

To make the problem analytically tractable, the derivation assumes conductors are perfect electric conductors of zero thickness, that the probe installation is such that there is no air gap between soil and sensor, and that the permittivity of the various media are purely real. Sources can be included by using a Fourier expansion in  $\phi$  and a Bessel expansion in  $r$ . The  $n, m$  mode refers to the  $m$  significant when the periodicity in  $\phi$  is integer  $n$ . The field components can be defined as follows:

$$E_z = AZ_n(k_c r) e^{-i\beta z - i n \phi} \quad (1)$$

$$H_z = BZ_n(k_c r) e^{-i\beta z - i n \phi} \quad (2)$$

$$E_\phi = -A \frac{n\beta}{k_c^2 r} Z_n(k_c r) + B \frac{i\omega\mu}{k_c} Z_n'(k_c r) \quad (3)$$

$$H_\phi = -A \frac{i\omega\epsilon}{k_c} Z_n'(k_c r) - B \frac{n\beta}{k_c^2 r} Z_n(k_c r) \quad (4)$$

$$E_r = -A \frac{i\beta}{k_c} Z_n'(k_c r) - B \frac{n\omega\mu}{k_c^2 r} Z_n(k_c r) \quad (5)$$

$$H_r = A \frac{n\omega\epsilon}{k_c^2 r} Z_n(k_c r) - B \frac{i\beta}{k_c} Z_n'(k_c r) \quad (6)$$

where  $E$  is the electric field,  $H$  is the magnetic field,  $A$  and  $B$  are constants,  $k_{c,i}$  are radial significant,  $\beta$  is the propagation constant,  $\epsilon$  is the permittivity,  $\mu$  is the permeability,  $Z_n$  is a Bessel function or a modified Bessel function and the type of Bessel function used depends on the sign of  $k_{c,i}^2$ . Negative  $k_{c,i}^2$  (that is, imaginary significant) necessitates the use of modified Bessel functions (meaning the fields decay approximately exponentially with radius) and positive  $k_{c,i}^2$  (real wavenumber) requires Bessel functions (meaning the fields decay approximately exponentially, but also oscillate with radius). For TE modes,  $A = 0$ ; for TM modes,  $B = 0$ ; and for hybrid modes, both  $A$  and  $B$  are nonzero. The  $k_c$  for each layer  $i$  are related to  $\beta$  by

$$k_{c,i}^2 = \omega^2 \mu_i \epsilon_i - \beta^2. \quad (7)$$

The boundary conditions of finite fields at  $r = 0$  and finite power at  $r = \infty$  force the Bessel function in the air-core layer to be  $I_n$  and to be  $J_n$  in the soil layer. The plastic layer admits either Bessel or modified Bessel functions, and of both type 1 and 2 (i.e.,  $C_1 I_n + C_2 K_n$  or  $c_1 J_n + c_2 Y_n$ ). This will, after application of the continuity boundary conditions (BCs) at the material layer interfaces, give a matrix equation of the form:

$$\mathbf{Q}\mathbf{c} = 0 \quad (8)$$

where  $c$  is a vector of the coefficients for each of the Bessel functions. The determinant of  $\mathbf{Q}$  must be zero to admit a non-trivial solution for  $c$ ;  $\det(\mathbf{Q}) = 0$  gives the characteristic equation to solve for the wavenumber at each mode. This equation can be solved numerically for  $\beta$ .  $\beta$  must be less than the TEM propagation constant for soil and larger than the TEM propagation constant for the air core [28]. Since in this case,  $\beta$  is a function of frequency even in the case of non-dispersive materials, the sensor will have material as well as waveguide dispersion. In the case where solution of the characteristic equation yields the same  $\beta$  for multiple modes, these modes are referred to as degenerate and are only counted once in the source expansion [23].

### A. Sources

Sources can be incorporated by using a modal expansion. At  $z = 0$ , having the center electrode carry a surface current of  $J_0$  and the adjacent electrodes carry  $-J_0/2$  can be described mathematically by the following expression for the z-directed surface current  $J$ :

$$J = \delta(r - b)J_0 \left( \text{rect} \left( \frac{\phi - \phi_1}{\phi_2 - \phi_1} \right) - \text{rect} \left( \frac{\phi - \phi_3}{\phi_4 - \phi_3} \right) / 2 - \text{rect} \left( \frac{\phi - \phi_5}{\phi_6 - \phi_5} \right) / 2 \right). \quad (9)$$

To use the modal expansion, the current must be related to the fields, which can be viewed as the sum of the fields for each mode. The modal sum is taken over all propagating modes at each frequency. The TE and TM modes don't propagate for the sensor surrounded by soil until the frequency exceeds 3-4 GHz; that is, there were no solutions to the wavenumber equation for frequencies below this range. Since the range of frequencies considered is governed by the bandwidth of the input pulse, and in this case, the spectral content is quite low above 3 GHz, the TE and TM modes are ignored

$$\vec{H} = \sum_{n=1, m=1}^{\infty} A_{nm} \vec{H}_{nm} \quad (10)$$

$$\vec{J} = \hat{r} \times \vec{H} \quad (11)$$

$$J_z = H_\phi \quad (12)$$

$$J_z = \sum_{n=1, m=1}^{\infty} A_{nm} \times \left( -\frac{\beta_{nm} n}{k_{c, nm}^2 r} c_8 Z_n(k_{c, nm} r) - \frac{i\omega\epsilon}{k_{c, nm}} c_7 Z_n'(k_{c, nm} r) \right). \quad (13)$$

Equating Eqs. 9 and 13, multiplying by  $e^{iN\phi} r^2 Z_N(k_{c, NM} r)$ , and integrating over  $\phi$  and  $r$ , one obtains:

$$A_{n, m} = \frac{b J_0 k_{c, nm} \alpha_{nm} Z_n(k_{c, nm} b)}{i n^2 \pi \beta_{c, nm} c_8 Z_n^2(\alpha_{nm})} \times \left( e^{in\phi_2} - e^{in\phi_1} - \frac{e^{in\phi_4} - e^{in\phi_3}}{2} - \frac{e^{in\phi_6} - e^{in\phi_5}}{2} \right) \quad (14)$$

where  $\alpha_{nm}$  is the  $m$ th root of the  $n$ th Bessel function.

### B. Sampling Area

The sampling area gives an indication of how much of the power propagated along the probe goes into the soil, and how far it penetrates into the soil surrounding the probe. As defined by [20], the weighting function is expressed in terms of the potential

$$w = \frac{|\nabla\Phi|^2}{\int \int |\nabla\Phi|^2 dA} \quad (15)$$

but since here we use the hybrid mode formulation, we define the weighting function in terms of the power  $\vec{P} = \frac{1}{2} \vec{E} \times \vec{H}^*$ :

$$w = \frac{P_z}{\int \int P_z dA}. \quad (16)$$

Since the fields are calculated at discrete points, even though the solution is in terms of analytical functions, the weights of each point ( $w_i$ ) are ranked in descending order and used to calculate the fractional contribution of the top  $N$  points:

$$f = \frac{100 \sum_1^N w_i A_i}{\sum_1^{N_{tot}} w_i A_i} \quad (17)$$

where  $N_{tot}$  is the total number of points. The area corresponding to the top points that contribute to  $f = 90\%$  in the soil is the sampling area:

$$A_{samp} = \sum_1^N A_i. \quad (18)$$

To evaluate the distribution of power between the probe and soil, we use the fraction of the total power in the soil:

$$f_{soil} = \frac{P_{soil}}{P_{tot}}. \quad (19)$$

So,  $A_{samp}$  is an indicator of the area of soil which contributes the most to the sensor reading, while  $f_{soil}$  is an indicator of the relative contribution of soil vs. probe.

### C. Waveform

Once the propagation constant  $\beta$  has been determined as a function of frequency, given an input voltage waveform  $V_{in}(t)$ , the output voltage waveform can be obtained. First,  $V_{in}(t)$  should be transformed into the frequency domain through the Fourier transform

$$V_{in}(\omega) = F\{V_{in}(t)\}. \quad (20)$$

Then, a phase factor corresponding to the longitudinal position  $z$  is added:

$$V(z, \omega) = V_{in}(\omega) e^{-j\beta(\omega)z}. \quad (21)$$

Assuming a physical probe length  $L$  and open circuit conditions at the probe end, the reflected wave should be incorporated; then the voltage is brought back into the time domain through the inverse Fourier transform:

$$V(z, t) = F^{-1} \left\{ V_{in}(\omega) \left( e^{-j\beta(\omega)z} + e^{-j2\beta(\omega)L} e^{j\beta(\omega)z} \right) \right\}. \quad (22)$$

The measured waveform is where  $z = 0$ . Losses can be incorporated by replacing  $-j\beta(\omega)$  with  $-a(\omega) - j\beta(\omega)$ .

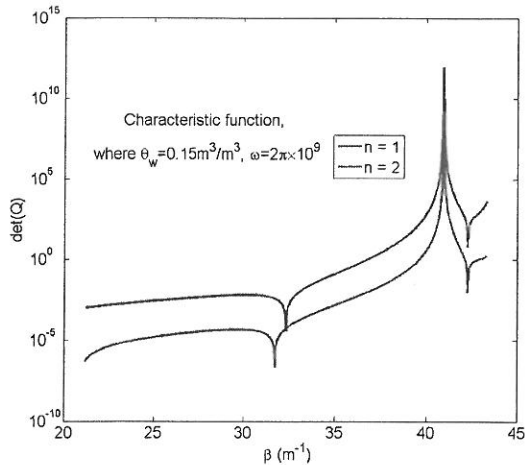


Fig. 2. Characteristic function at different  $n$  values, for fixed  $\theta_w$  and  $\omega$ .

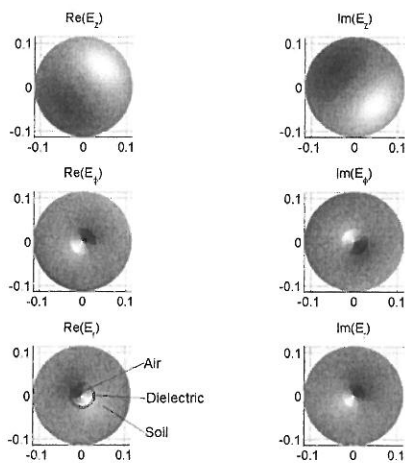


Fig. 3. Electric field components of HE11 mode corresponding to the characteristic equation in Fig. 2.

### III. RESULTS

The analytical development in the preceding section was implemented in MATLAB.<sup>1</sup> Soil permittivity was calculated using the model of [25] and the permittivity of the plastic tube substrate was assumed homogeneous and frequency-invariant. The fields were calculated at points on a cylindrical mesh using the expressions for each of the field components, after solving the characteristic equation using the MATLAB built-in root-finding routines. Fig. 2 shows an example of the characteristic equation as a function of propagation constant. Figure 3 shows the real and imaginary components of the electric field for the HE11 mode corresponding to the characteristic equation plotted in Fig. 2. These fields demonstrate the double-peaked intensity distribution of a HE11 mode in hollow optical fibers [24].

<sup>1</sup>The mention of trade names of commercial products in this article is solely for the purpose of providing specific information and does not imply recommendation or endorsement by the U.S. Department of Agriculture.

TABLE I  
DEFAULT SENSOR PARAMETERS

Soil water content	$\theta_w$ ( $m^3/m^3$ )	0.15
Cylinder radius	$a$ (m)	0.0254
Cylinder thickness	$\Delta r$ (m)	0.0032
Electrode spacing	$\phi = \phi_3 - \phi_1$ (rad)	$\pi/4$
Electrode width	$\Delta\phi = \phi_3 - \phi_2$ (rad)	$\pi/16$
Cylinder dielectric	$\epsilon_{pvc}$ (-)	3.18
Probe length	$L$ (m)	0.2
Frequency	$\omega$ (rad/s)	$2\pi \times 10^9$

The following subsections use the MATLAB routines to investigate the impacts of the soil water content and sensor geometry on the sensor performance, in terms of the sampling area and the waveform. Soil water content, cylinder radius, cylinder thickness, cylinder dielectric, electrode spacing, and electrode width were swept individually; in the case of these sweeps, the frequency was held constant at 1 GHz. Unless otherwise specified by the variable sweep, the parameters describing the sensor are as given in Table I. The input waveform had the form of

$$V_{in}(t) = 1 - e^{-t/\tau} \quad (23)$$

where  $\tau = 150$  ps. This waveform was discretized with 256 points and a sampling interval of 50 ps and brought into the frequency domain through the Fast Fourier Transform. After calculating the fields at each frequency, it was brought back into the time domain as in Eq. 22 through the inverse FFT. Aside from some periodicity, which is an artefact of using a discrete Fourier transform, this gives the waveform that would be used to estimate the delay time for determining the permittivity. For clarity, we plot the waveform for a time window that excludes the artefacts near  $t = 0$ .

Soil dielectric properties were incorporated using the model of [25] and using the soil textural properties of the Pullman Bt soil in [29].

#### A. Effect of Soil Water Content

Fig. 4 shows the effect of soil water content on sampling area and on  $f_{soil}$ . As soil water content increases, the permittivity of the soil increases. Below around  $\theta_w = 0.15 m^3/m^3$ , the soil permittivity is less than the probe substrate permittivity; where this is the case, the wave propagation is as a guided (non-radiating) mode within the plastic tube substrate material. In this case, decreasing soil permittivity relative to substrate permittivity requires greater  $\beta$  to satisfy the boundary conditions between the media. Larger  $\beta$  leads to lower  $k_c^2$  for the substrate region, which leads to more slowly changing Bessel functions, so more power is confined in the substrate region rather than the soil region. When the soil permittivity exceeds the substrate permittivity, the resulting  $k_c^2$  (see Eq. 7) for the soil region is positive, and negative for the air and substrate regions. As  $\epsilon_{soil}$  increases, the  $k_c$  in the soil increases; this makes the Bessel functions in this region decay more quickly with increasing  $r$ . Therefore, the most power is

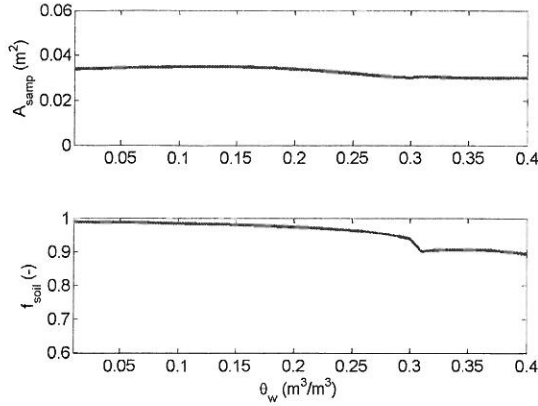


Fig. 4. Sampling area and fraction of total power in soil as related to soil water content.

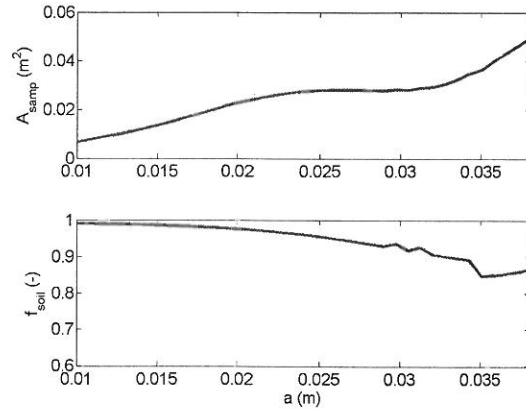


Fig. 6. Sampling area and fraction of total power in soil as related to radius.

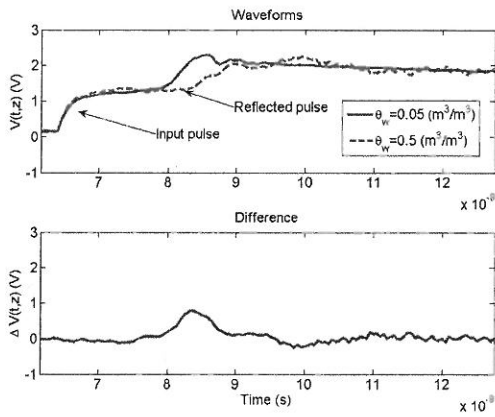


Fig. 5. Voltage waveform at two different soil water content values.

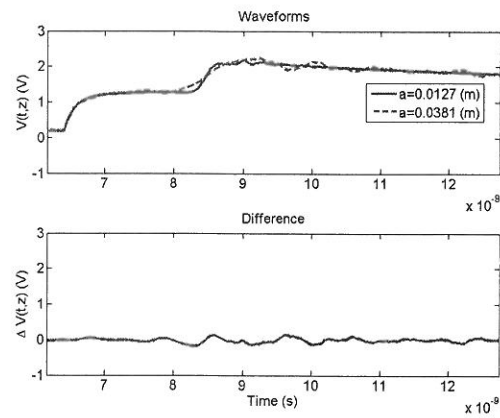


Fig. 7. Voltage waveform at two different radius values.

confined into a smaller region, so the sampling area is smaller as soil water content increases.

Fig. 5 demonstrates the effect of soil water content on voltage waveform. Soil dielectric varies more strongly with frequency at higher water content levels, leading to greater dispersive effects at soil water content values. Higher permittivities of higher water content soil makes the travel time longer, so the waveform delay is longer when the soil water content is greater.

**B. Effect of Probe Design**

1) *Cylinder Radius*: Fig. 6 shows the effect of access tube radius on sampling area and on  $f_{soil}$ . Increasing  $r$  increases the electrode separation, which leads to increased sampling area as found by [20] for the cylindrical probe of [10]. However, the fraction of total power in the soil decreases with increasing radius because  $k_c^2$  gets more negative as  $\beta$  increases with increasing  $a$ , and the Bessel functions inside the air core are steeper, so greater power is confined in this region.

Fig. 7 demonstrates the effect of tube radius on the voltage waveform. Where  $r$  is greater, there is more dispersion, as

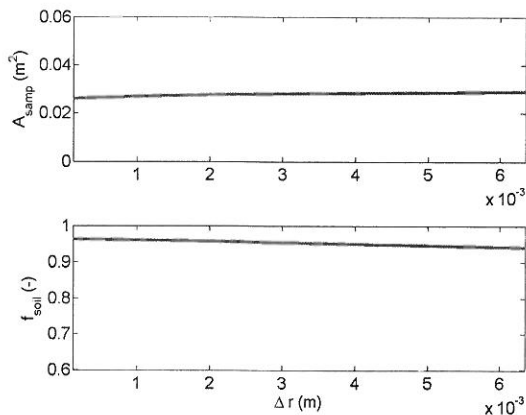


Fig. 8. Sampling area and fraction of total power in soil as related to cylinder thickness.

increasing  $r$  necessitates a smaller  $\beta$  in order to satisfy boundary conditions. Because  $\beta$  is smaller, the relative impact of changes in properties is greater, leading to greater dispersion and potential ambiguity of the TDR signal.

2) *Cylinder Thickness*: Fig. 8 shows the effect of probe substrate (tube) thickness on sampling area and on  $f_{soil}$ .

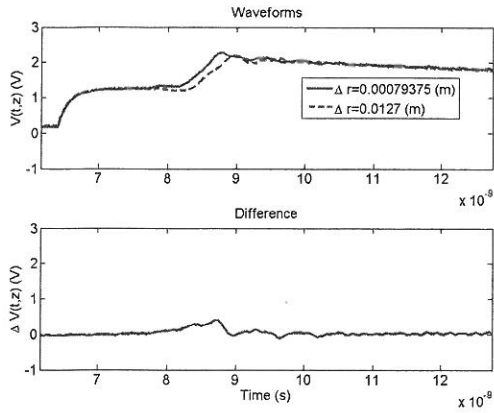


Fig. 9. Voltage waveform at two different thickness values.

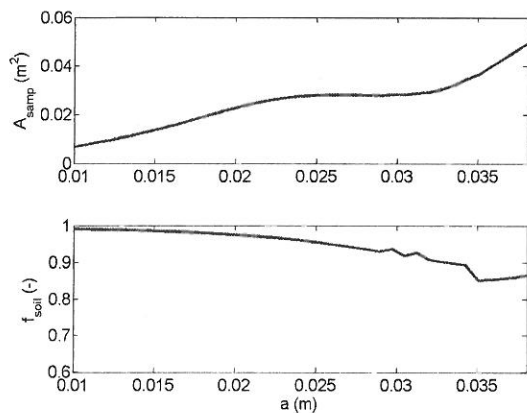


Fig. 10. Sampling area and fraction of total power in soil as related to radius, with constant electrode separation.

Similar to the effect of increasing  $r$ , increasing the thickness increases the electrode separation, which leads to increased sampling area, and decreasing  $f_{soil}$ .

Fig. 9 demonstrates the effect of tube thickness on voltage waveform. The impact is smaller but still present, similar in nature and cause to the effect of  $r$ .

3) *Electrode Spacing*: The response of sampling area and of  $f_{soil}$  to the angle between the electrode is relatively flat. As in the previous sections, increasing angle increases separation, which increases sampling area very slightly. However, the effect of  $\phi$  is only related to the source distribution, not the wavenumber, as  $\phi$  has no bearing on the characteristic equation (necessarily a byproduct of the assumption of the hybrid mode propagation).

Since in theory,  $\phi$  has no effect on  $\beta$ , the dispersive effects and travel time are identical for all  $\phi$  values.

4) *Cylinder Radius and Thickness at Constant Electrode Separation*: To isolate the effects of tube geometry and electrode separation, the electrode angle was adjusted to maintain constant separation while varying the radius or thickness independently.

Fig. 10 shows the effect of access tube radius on sampling area and on  $f_{soil}$ , when electrode separation is held constant.

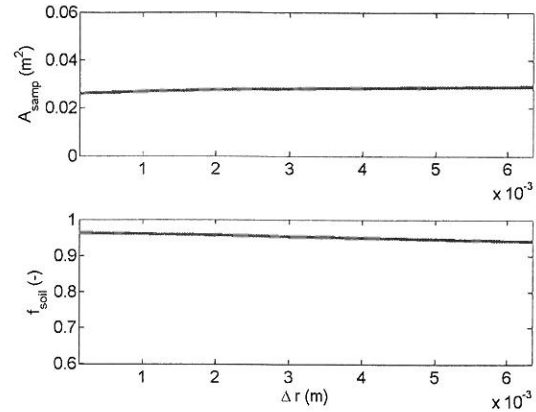


Fig. 11. Sampling area and fraction of total power in soil as related to cylinder thickness, with constant electrode separation.

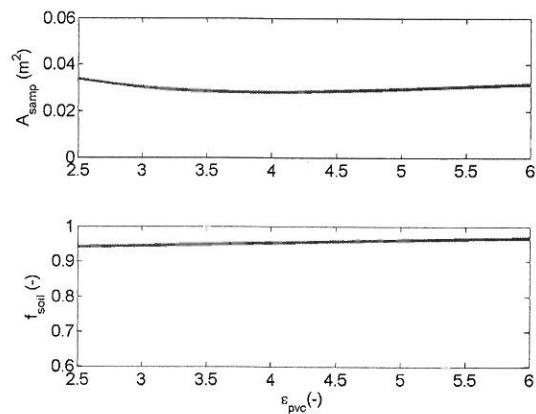


Fig. 12. Sampling area and fraction of total power in soil as related to cylinder dielectric.

Fig. 11 shows the effect of probe substrate (tube) thickness on sampling area and on  $f_{soil}$ , when electrode separation is held constant. In both cases, the trend is nearly identical to the trend in the case when the electrode separation varies, indicating that the increase in sampling area is due to the increase in radius independent of electrode separation. This could be because as  $r$  increases, the  $\beta$  required to satisfy the boundary conditions decreases and levels out around  $r = 0.0125$  m. Smaller  $\beta$  means a larger  $k_c^2$ , which would seem to indicate a more sharply decaying Bessel function and thus a smaller sampling area; however, since the radius is also increasing, and Bessel functions are less steep at larger arguments, the overall effect is that of a more slowly decaying function in the radial direction, leading to a larger sampling area.

5) *Electrode Width*: Sampling area is relatively insensitive to  $\Delta\phi$ , for similar reasons to those given for the effect of  $\phi$ . As  $\Delta\phi$  is only related to the source distribution, not the wavenumber, it has no effect on the dispersion and travel time.

6) *Cylinder Dielectric*: Fig. 12 shows the effect of the tube substrate permittivity on sampling area and on  $f_{soil}$ . The sampling area is relatively insensitive to the plastic substrate

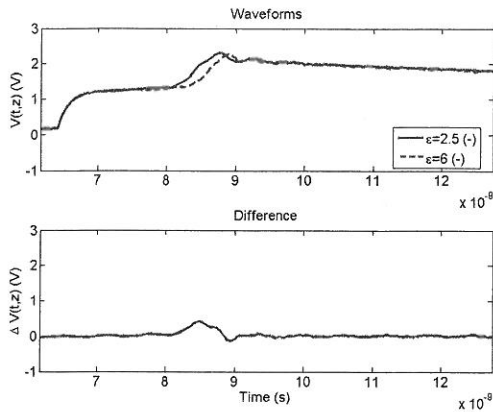


Fig. 13. Voltage waveform at two different dielectric values.

dielectric, outside of a small region where  $\epsilon_{pvc}$  is between  $\epsilon_{soil}$  and  $\epsilon_{air}$ . The minimum sampling area occurs where  $\epsilon_{pvc}$  is roughly  $\epsilon_{soil}$ . Before this point, the cylinder dielectric is less than the the soil dielectric, leading to unguided modes inside the substrate. After this point, the modes are guided within the substrate, which require increasingly large  $\beta$  to satisfy the boundary conditions between the adjacent media. As  $\beta$  increases, the  $k_c^2$  of the soil region decreases; lower  $k_c^2$  means the Bessel functions decay more slowly, leading to more power in the soil region.

Fig. 13 demonstrates the effect of tube dielectric constant on voltage waveform. The delay is slightly higher with higher cylinder dielectric.

#### IV. CONCLUSION

The performance of a cylindrical access-tube TDR probe was estimated using an analytical derivation of the hybrid propagating modes. It was found that when the soil and tube substrate have identical dielectrics, then sampling area has a local minimum. Tube radius has the largest impact of any geometrical parameter on sampling area. Electrode separation angle increases the sampling area slightly. The effects on waveform are greatest for soil water content, cylinder dielectric, and tube radius: where increasing any of these increase delay and dispersion. Further studies will investigate the performance of sensor prototypes. These conclusions and modal field solutions, if in agreement with prototype sensor performance, may be used in future studies for design optimizations of the sensor in different soils.

#### REFERENCES

- [1] J. Merriam, "A management control concept for determining the economical depth and frequency of irrigation," *Trans. Amer. Soc. Agric. Eng.*, vol. 9, no. 4, pp. 492–498, 1966.
- [2] T. Jackson and T. Schmugge, "Passive microwave remote sensing system for soil moisture: Some supporting research," *IEEE Trans. Geosci. Remote Sens.*, vol. 27, no. 2, pp. 225–235, Mar. 1989.
- [3] S. Evett, L. Heng, P. Moutonnet, and M. Nguyen, "Field estimation of soil water content: A practical guide to methods, instrumentation and sensor technology," International Atomic Energy Agency, Vienna, Austria, Tech. Rep. IAEA-TCS-30, 2008.
- [4] N. Mazahrih, N. Katbeh-Bader, S. Evett, J. Ayars, and T. Trout, "Field calibration accuracy and utility of four down-hole water content sensors," *Vadose Zone J.*, vol. 7, no. 3, pp. 992–1000, 2008.
- [5] S. Evett and J. Steiner, "Precision of neutron scattering and capacitance type soil water content gauges from field calibration," *Soil Sci. Soc. Amer. J.*, vol. 59, no. 4, pp. 961–968, 1995.
- [6] S. Evett, R. Schwartz, J. Tolck, and T. Howell, "Soil profile water content determination: Spatiotemporal variability of electromagnetic and neutron probe sensors in access tubes," *Vadose Zone J.*, vol. 8, no. 4, pp. 926–941, 2009.
- [7] G. Topp, J. Davis, and A. Annan, "Electromagnetic determination of soil water content: Measurements in coaxial transmission lines," *Water Resources Res.*, vol. 16, no. 3, pp. 574–582, 1980.
- [8] H. Nissen, P. Moldrup, T. Olesen, and P. Raskmark, "Printed circuit board time domain reflectometry probe: Measurements of soil water content," *Soil Sci.*, vol. 164, no. 7, pp. 454–466, 1999.
- [9] T. Heimovaara, "Design of triple-wire time domain reflectometry probes in practice and theory," *Soil Sci. Soc. Amer. J.*, vol. 57, no. 6, pp. 1410–1417, 1993.
- [10] J. Redman and S. DeRyck, "Monitoring non-aqueous phase liquids in the subsurface with multilevel time domain reflectometry probes," in *Proc. Symp. Workshop Time Domain Reflect. Environ. Infrastruct. Mining Applicat.*, Evanston, IL, Sep. 1994, pp. 7–8.
- [11] S. Evett, "The TACQ computer program for automatic time domain reflectometry measurements: I. Design and operating characteristics," *Trans. ASAE*, vol. 43, no. 6, pp. 1939–1946, 2000.
- [12] W. Hook, N. Livingston, Z. Sun, and P. Hook, "Remote diode shorting improves measurement of soil water by time domain reflectometry," *Soil Sci. Soc. Amer. J.*, vol. 56, no. 5, pp. 1384–1391, 1992.
- [13] R. Friel and D. Or, "Frequency analysis of time-domain reflectometry (TDR) with application to dielectric spectroscopy of soil constituents," *Geophysics*, vol. 64, no. 3, pp. 1–3, 1999.
- [14] B. Raphael and I. Smith, *Fundamentals of Computer-Aided Engineering*. New York: Wiley, 2003.
- [15] J. J. Casanova, Z. N. Low, J. Lin, and R. Tseng, "Transmitting coil achieving uniform magnetic field distribution for planar wireless power transfer system," in *Proc. Radio Wireless Symp.*, San Diego, CA, 2009, pp. 530–533.
- [16] A. Annan, "Time-domain reflectometry air-gap problem for parallel wire transmission lines," Geological Survey of Canada, Ottawa, ON, Canada, Tech. Rep. 77-1B, 1977, pp. 59–62.
- [17] J. Knight, P. Ferré, D. Rudolph, and R. Kachanoski, "A numerical analysis of the effects of coatings and gaps upon relative dielectric permittivity measurement with time domain reflectometry," *Water Resources Res.*, vol. 33, no. 6, pp. 1455–1460, 1997.
- [18] J. Knight, "Sensitivity of time domain reflectometry measurements to lateral variations in soil water content," *Water Resources Res.*, vol. 28, no. 9, pp. 2345–2352, 1992.
- [19] P. Ferré, D. Rudolph, and R. Kachanoski, "Spatial averaging of water content by time domain reflectometry: Implications for twin rod probes with and without dielectric coatings," *Water Resources Res.*, vol. 32, no. 2, pp. 271–279, 1996.
- [20] P. Ferré, J. Knight, D. Rudolph, and R. Kachanoski, "The sample areas of conventional and alternative time domain reflectometry probes," *Water Resources Res.*, vol. 34, no. 11, pp. 2971–2979, 1998.
- [21] M. Schwank, T. Green, C. Matzler, H. Benedickter, and H. Fluhler, "Laboratory characterization of a commercial capacitance sensor for estimating permittivity and inferring soil water content," *Vadose Zone J.*, vol. 5, no. 3, pp. 1048–1064, 2006.
- [22] C. Balanis, *Advanced Engineering Electromagnetics*. New York: Wiley, 1989.
- [23] K. Okamoto, *Fundamentals of Optical Waveguides*. New York: Academic, 2006.
- [24] S. Lee, J. Park, Y. Jeong, H. Jung, and K. Oh, "Guided wave analysis of hollow optical fiber for mode-coupling device applications," *Lightw. Technol. J.*, vol. 27, no. 22, pp. 4919–4926, 2009.
- [25] R. Schwartz, S. Evett, M. Pelletier, and J. Bell, "Complex permittivity model for time domain reflectometry soil water content sensing: I. Theory," *Soil Sci. Soc. Amer. J.*, vol. 73, no. 3, pp. 886–897, 2009.
- [26] D. Pozar, *Microwave Engineering*. New York: Wiley, 2009.
- [27] D. Kirkby, "Finding the characteristics of arbitrary transmission lines," *Amateur Radio J. QEX*, pp. 3–10, Dec. 1996.
- [28] J. Buck, *Fundamentals of Optical Fibers*. New York: Wiley, 2004.
- [29] R. Schwartz, S. Evett, and J. Bell, "Complex permittivity model for time domain reflectometry soil water content sensing: II. Calibration," *Soil Sci. Soc. Amer. J.*, vol. 73, no. 3, pp. 898–909, 2009.



**Joaquin Casanova** (S'05–M'09) received the B.S. and M.S. degrees in agricultural and biological engineering and the Ph.D. degree in electrical engineering from the University of Florida, Gainesville, in 2006, 2007, and 2010, respectively.

He is currently with USDA-Agricultural Research Service, Bushland, TX, researching electromagnetic soil moisture sensors. His previous research included microwave remote sensing of agricultural systems and wireless power transfers.

Dr. Casanova is a member of the American Society of Agricultural and Biological Engineers.



**Steve Evett** received the Graduate degree from the University of Idaho, Moscow, and the University of Arizona, Tucson, and was raised on an irrigated dairy farm in Southern Idaho.

He is a Research Soil Scientist with USDA-Agricultural Research Service, Bushland, TX, Conservation and Production Research Laboratories, Bushland. He uses field measurements, electronic sensing and automation systems, and energy and water balance models to study irrigated crop water use, irrigation methods and automation as they

affect crop water productivity, as well as water content sensing methods used

to control irrigation and to quantify crop water use. In addition to research locations in the U.S., he has active research projects in the Middle East and Uzbekistan on crop water use, irrigation scheduling and soil water measurement, and he has worked in China, Egypt, Jordan, and the U.S., to build and use weighing lysimeters to measure crop water use. Since 2003, he has been the ARS Research Coordinator for the Middle East Regional Irrigation Management Information Systems Project, which has research and extension partners in Israel, Jordan, and the Palestinian Authority.

Dr. Evett is a fellow of the Soil Science Society of America and the American Society of Agronomy. He has received the Soil Science Society of America Applied Soil Science Research Award, the U.S. Department of Energy Federal Energy and Water Management Award, and the USDA-ARS Technology Transfer Award. He is a past President of the Texas Council of Chapters of the Soil and Water Conservation Society, a past Associate Editor of the *Agronomy Journal*, and currently serves as an Associate Editor of the *Vadose Zone Journal* and on the Editorial Board of *Agricultural Water Management*.

**Robert Schwartz** received the Ph.D. degree in soil physics from Texas A&M University, College Station, in 1998.

He has been a Research Soil Scientist with USDA-Agricultural Research Service, Bushland, TX, since 1998. His current and past research interests include inverse estimation of soil hydraulic and dispersive transport properties, influence of soil physical properties on soil water balance, and characterization of soil dielectric properties for electromagnetic soil water content sensing.